Measurement and Modeling of the Effects of Transcranial Magnetic Stimulation on the Brain

Oluwaponmile F. Afuwape [1,2], Hiroyuki Oya, MD [3], Aaron D. Boes, MD [4], David C. Jiles [1], *Life Fellow, IEEE*

[1] Department of Electrical and Computer Engineering, Iowa State University, Ames, IA 50011, USA
[2] Department of Mechanical Engineering, Iowa State University, Ames, IA 50011, USA
[3] Department of Neurosurgery, University of Iowa, Iowa City, IA 52242, USA
[4] Department of Neurology, University of Iowa, Iowa City, IA 52242, USA.

Transcranial Magnetic Stimulation (TMS) is a method of non-invasively modulating the excitability of the brain. TMS relies on the principle of electromagnetic induction in producing an electric field that stimulates neurons. Measuring the effect of TMS in real time and being able to determine its spatiotemporal resolution increase its potential in both research and clinical applications. In this paper, the authors model the electric fields of three TMS coils: Quadruple Butterfly Coil (QBC), Triple Halo Coil (THC) and the Magventure B65 coils, by performing computational finite element (FE) analysis using the Sim4life software. To evaluate the accuracy of the electromagnetic models, we devised a novel experimental protocol that compares the maximum field intensity stimulated using modeling with the induced voltage experimentally measured within a phantom brain in response to TMS.

***Index Terms*— computational finite element (FE) analysis, electromagnetic coils, gel-based phantom, Transcranial Magnetic Stimulation (TMS).**

I. Introduction

Transcranial Magnetic Stimulation (TMS) is a non-invasive method of electrically stimulating the brain. It involves the use of time varying magnetic field generated from electromagnetic coils in inducing electric field in the brain [1]. TMS does not require surgery or anesthesia, thus providing a minimally invasive method of modulation. It has been used as a tool in neuroscience and increasingly as a treatment to patients with depression that do not respond to medications [3], [4].

With ongoing developments in TMS technology, the versatility of TMS is certain to increase. One area of TMS research aimed at greater versatility is the development of electromagnetic coils that are able to deliver more focal stimulation or coils that stimulate at a greater depth. There have been several designs proposed for the coils used in TMS [5], [6] to achieve higher focality and deeper penetration of the magnetic fields, with some already been commercially available like the figure of eight coil [7], [8]. A novel coil with increased focality is the Quadruple Butterfly coil (QBC) [9], and a coil capable of reaching deeper brain structures is the Triple Halo Coil (THC) [10]. The Magventure B65 coil is designed by [11] and also commercially available.

A clear understanding of the temporal and spatial resolution of both standard and novel TMS coils on the human brain would inform the optimal use of TMS for research and clinical applications. In the present research, the authors evaluate the performance of electromagnetic modeling of electric fields of three coils in a gel-based phantom. We hypothesize that accurately modeling the electromagnetic fields of these coils can be used to predict induced voltage measured using intracranial electrodes embedded in a gel-based phantom, and further, that these results would help to determine the safety of using novel TMS coils in the human brain.

To test this hypothesis, we model the magnetic fields of the Quadruple Butterfly Coil (QBC), Triple Halo Coil (THC) and the Magventure B65 coils by performing computational finite element (FE) analysis using the Sim4life software [12]. To test these models, we use a novel experimental paradigm that involves calculating the induced electric field intensity (E-Field) in the gel phantom and comparing it to the predictions generated using the models. Specifically, the induced differential voltage in the gel phantom were measured at different points by using intracranial electrodes and measurements were compared with results from the FE analysis as a test for the precision of our electromagnetic modeling.

The experimental paradigm for measuring the effects of TMS on the gel phantom with intracranial electrode and comparison with simulation results employed in this research would be vital information for further development and assessment of the novel coil design for future clinical applications.

II. Method

A. Finite Element Simulation

Sim4Life software, an electromagnetic quasi-static low frequency solver [12], was used to simulate the experimental model. A gel phantom was modelled with dimensions 200x200x200 mm and the electrical conductivity and relative permittivity of the gel phantom was specified as confirmed with literature values [13], [14]. The Sim4Life software was used to simulate a single pulse of current of amplitude 5000 A and an operational frequency of 2500 Hz was inputted for each coil. With the origin (0,0,0) at the center of the surface of the gel phantom, the QBC and B65 coils were positioned at a distance of 10 mm above the surface of the gel phantom to account for both the insulation of the coils and the thickness of the

container. The THC, because of its configuration, was positioned just at a distance of 100 mm on the vertical center from the origin of the gel phantom. The setup of these coils in the finite element simulations are represented in the Fig. 1 below.

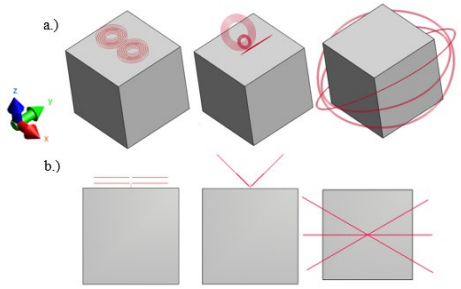

Fig. 1. a.) 3D perspective view of the setup with the B65 Coil, QBC and THC. This arrangement was used in the finite element simulation (figure has been tilted to give a better understanding of the arrangement). The coordinate system is such that the positive Z-axis is projected upwards from the center of the surface of the gel phantom. b.) Coronal view of the setup.

B. Experimental Method

A gel phantom made from Polyacrylic acid (PAA) gel was fabricated according to the ASTM (American Society for Testing and Materials, 2011) standards section F2182 [13], [14] which is the standard test method for medical devices. The gel phantom is made from Sodium Chloride (NaCl), Polyacrylic acid and water. The electrical properties of the PAA gel is reflected in the Table 1.

Table 1: Electrical Properties of Gel Phantom

Electrical Conductivity	0.47 S/m
Relative Permittivity	80

The gel phantom was placed in a custom-made container. The container was made with polymethyl methacrylate (PMMA) sheets of dimension 203x203x203 mm (8x8x8 inches) and a wall thickness of 4.76 mm (3/16 inches). A 32 contact grid electrodes (model number FG32C-SP10X-000) sourced from Ad-Tech Medical Instrument Corporation [15] was used to measure the induced differential voltage readings from the experimental setup. The grid electrode is made of Platinum-Iridium disk contacts with an exposed disk diameter of 2.3 mm and a 10 mm spacing between each contact and with an in-situ impedance of 1.0 – 3.0 kOhm at 1 kHz. Basically, the intracranial electrode was used to probe the differential voltage generated by the TMS induced E-field. The differential voltages were measured between adjacent contacts of the intracranial electrode at different vertical (Z-axis) and horizontal distances (X- and Y- axis) and visualized using an oscilloscope (Tektronix TDS2022, 200MHz Bandwidth). A Magventure, Magvita TMS Cool B65 coil was placed at the base of the container for ease of setup and was used for the stimulation of the gel phantom. This coil was able to deliver stimuli of over 40 Hz repetition rate and a maximum initial magnetic flux density of 36 kT/s when operated at 100%. This B65 coil has a 2 x (2 x 5) number of windings, inner diameter of 1.4 in (35 mm), outer diameter of 3 in (75 mm) and a winding height of 0.5 in (12 mm) [11]. The induced voltage readings were taken with the stimulator operating at 100% output. The experimental setup and the positioning of the coil is represented in Fig. 2.

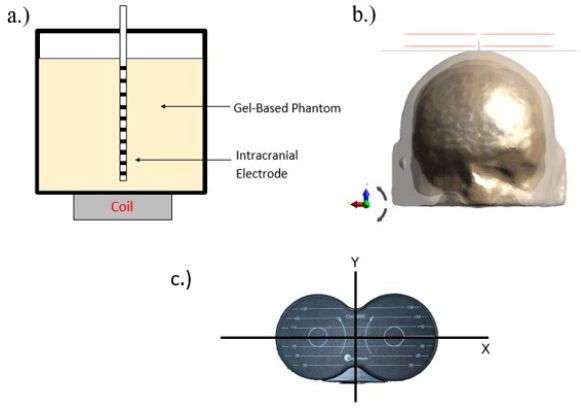

Fig. 2. Experimental setup and positioning of the B65 coil on the gel phantom Fig. a.) Coil positioning with the center of the gel aligning with the center of the B65 coil. b.) Positioning of the B65 coil over a head model when TMS is administered. c.) Coordinate of the B65 coil with the X- and Y- axis of the coil aligning with that of the gel phantom.

III. Results And Discussion

The B65 coil and gel phantom was modeled and the induced electric field within the gel phantom were extracted. The induced electric field values were extracted at the origin (0,0,0) and at different vertical (Z-axis) and horizontal distances (X- and Y- axis) in the gel phantom. The readings were taken such that on the coronal plane (XZ-plane) and the longitudinal plane (YZ-plane), measurements at 10, 20, 30 and 40 mm away from the center of gel phantom on the X-axis and Y-axis, and at every 10 mm vertically downwards on the Z-axis were extracted. The induced electric field values from the simulation are presented in Table 2.

Table 2. Induced Electric Field (E-Field, V/m) from simulations conducted with the B65 coil. The Z-distance is measured from the bottom face of the coil vertically downward into the gel phantom such that a distance of 10 mm corresponds to the location Z = 0 on the axis.

Induced Electric Field (V/m) from simulations using the B65 coils					
	X (mm)				
Z (mm)	0	10	20	30	40
10	132.93	126.12	102.31	61.52	15.69
20	84.53	79.62	64.69	41.17	13.48
30	54.74	51.53	42.16	27.86	10.98
40	36.06	34.00	28.08	19.14	8.57
50	24.10	22.77	18.97	13.25	6.44
60	16.27	15.40	12.92	9.18	4.67
70	11.04	10.46	8.81	6.31	3.25
	Y (mm)				
Z (mm)	0	10	20	30	40
10	132.93	124.29	102.15	75.69	52.75
20	84.53	80.39	69.38	54.97	40.84
30	54.74	52.59	46.74	38.69	30.19
40	36.06	34.88	31.63	26.99	21.84
50	24.10	23.43	21.54	18.80	15.62
60	16.27	15.87	14.75	13.08	11.10
70	11.04	10.80	10.12	9.09	7.85

Fig. 3 shows a graph of the induced electric field along the coronal plane and at a 10, 20, 30 and 40 mm distance away from the origin on the X-axis.

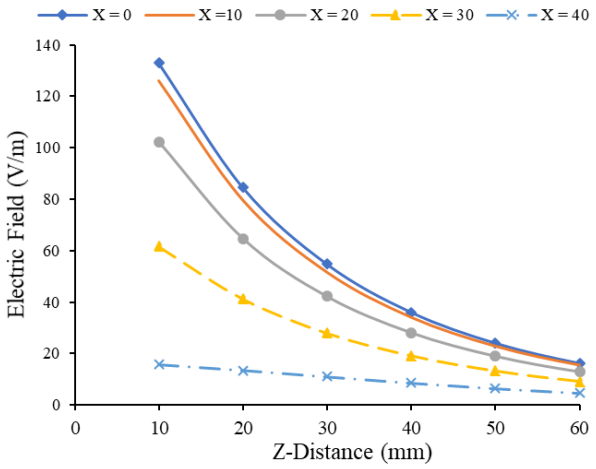

Fig. 3: Induced electric field (V/m) (from simulation with the B65 coil) on the coronal plane.

Fig. shows a graph of the induced electric field along the longitudinal plane and at a 10, 20, 30 and 40 mm distance away from the origin on the Y-axis.

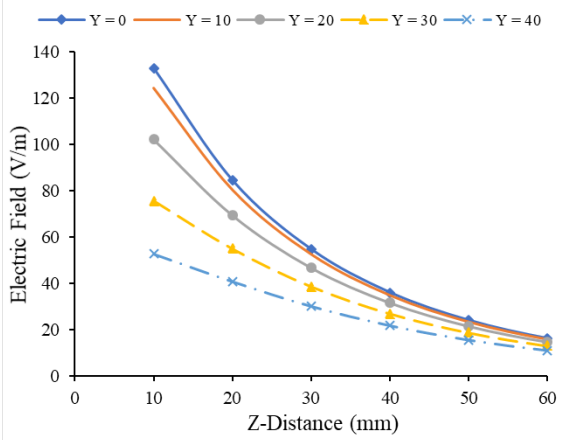

Fig. 4. Induced electric field (V/m) (from simulation with the B65 coil) on the longitudinal plane.

For the experimental result, the induced differential voltage was measured at the origin (0,0,0) and at different vertical (Z-axis) and horizontal distances (X- and Y- axis) in the gel phantom. The readings were taken such that on the coronal plane (XZ-plane), measurements at a distance of 10, 20, 30 and 40 mm away from the center of gel phantom on the X-axis and at every 10 mm vertically downwards on the Z-axis were recorded. The Z-axis distance accounted for the differential voltage readings at each of the adjacent contact points in the intracranial electrode. Likewise, the same method was employed in recording measurements along the longitudinal plane (YZ-plane). The induced voltage measurements from the experiment are reported in
Table .

Table 3. Induced Voltage measurements from experiments conducted with the B65 coil. The Z-distance is measured from the bottom face of the coil vertically downward into the gel phantom such that a distance of 10 mm corresponds to the location Z = 0 on the axis.

Differential Induced Voltage (V) readings on Grid Disk Intracranial Electrode (32 Channel) at 100% Stimulator Output					
	X (mm)				
Z (mm)	0	10	20	30	40
10	4.56	3.44	2.76	1.66	1.10
20	2.12	1.56	1.26	0.94	0.68
30	1.28	1.14	0.92	0.76	0.63
40	1.00	0.94	0.86	0.66	0.63
50	0.86	0.82	0.80	0.62	0.60
60	0.78	0.78	0.74	0.60	0.58
70	0.76	0.76	0.74	0.58	0.58
	Y (mm)				
Z (mm)	0	10	20	30	40
10	4.56	3.80	2.80	1.74	0.90
20	2.12	1.80	1.60	1.04	0.80
30	1.28	1.24	1.10	0.82	0.75
40	1.00	0.96	0.94	0.74	0.70
50	0.86	0.76	0.70	0.70	0.64
60	0.78	0.70	0.70	0.68	0.60
70	0.76	0.68	0.68	0.64	0.60

Fig. 5 shows the induced differential voltage along the coronal (XZ-) plane of the gel phantom and also at a 10, 20, 30 and 40 mm distance away from the origin on the X-axis. On this graph, we see a decline in the readings as the distance increases along the Z-axis. Along the X-axis, we also see a decline as the measurements moves away from the center of the gel phantom.

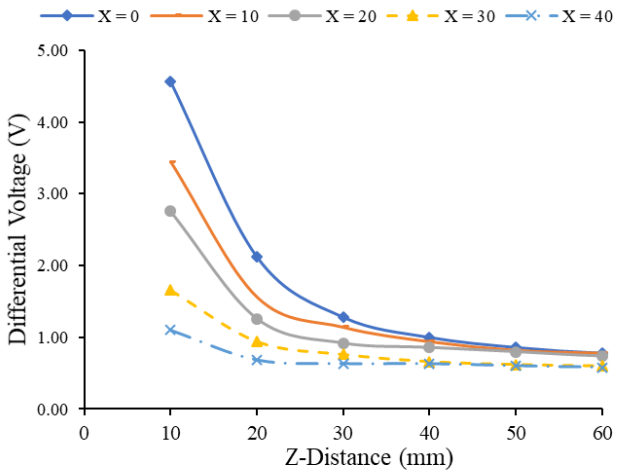

Fig. 5. Induced differential voltage (from experimental data using the B65 coil) on the coronal plane.

Fig. 6 shows the induced differential voltage along the longitudinal plane (YZ-) of the gel phantom and also at every 10 mm distance away from the origin on the Y-axis. On this graph, we see a decline in the values as the distance increases along the Z-axis just like the plot on the coronal plane. Along

This article has been accepted for publication in a future issue of this journal, but has not been fully edited. Content may change prior to final publication. Citation information: DOI 10.1109/TMAG.2020.3008554, IEEE Transactions on Magnetics

the Y-axis, we also see a decline as the measurements move away from the center of the gel phantom.

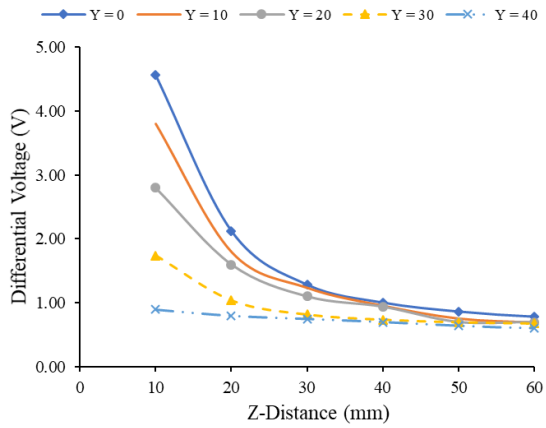

Fig. 6. Induced differential voltage (from experimental data using the B65 coil) on the longitudinal plane.

Looking at the induced differential voltage on both the coronal and longitudinal plane (Fig. 5 and Fig. 6), we see that the graphs both exhibit a decline as the distance along the Z-axis increases. This decline is expected according to the Biot-Savart Law but we expect that the curve be exponential and not to flatten out from the position of Z = 50 mm. We hypothesize that this might be due to the increased potential at the electrode/gel interface.

A linear regression model was developed to estimate the correlation between the E-field from simulations and the induced differential voltage from experiments. With the regression analysis, R-square value of 0.873 (P-Value < 3.80 e-10) was obtained.

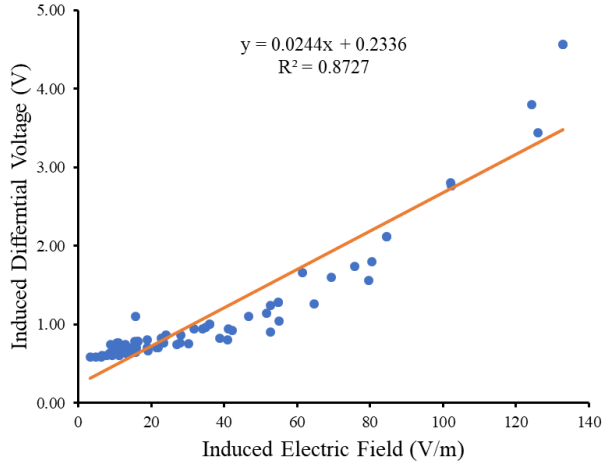

Fig. 7. Graph showing correlation between the electric field (V/m) extracted from simulation and induced differential voltage (V) measured from experiments.

To better understand the distribution of the induced electric field by the B-65 coils, Fig. 8 illustrates the electric field profile along the X-axis. A triple lobe structure is observed in Fig. 8 and this is because of the geometry and configuration of the B65 coil. It is observed that along the X-axis from the center at X = 0 mm, the gel is induced with the highest electric field. The induced electric field begins to decrease at both the negative X- and positive X- direction until X = 50 mm and then starts to increase again at X = 60 mm till it peaks at X = 80 mm and then resumes its downward decline until X = 100 mm.

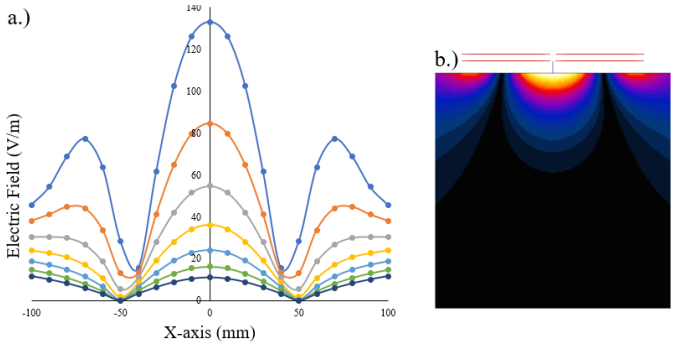

Fig. 8. a.) A triple lobe structure is observed on the electric field profile of the B65 coil in the X-axis. b.) Slice view along the coronal plane of the gel phantom.

The electric field profile along the Y-axis is illustrated in Fig. 9. As expected, the gel is induced with the highest electric field at the center and decreases in both direction of the Y-axis.

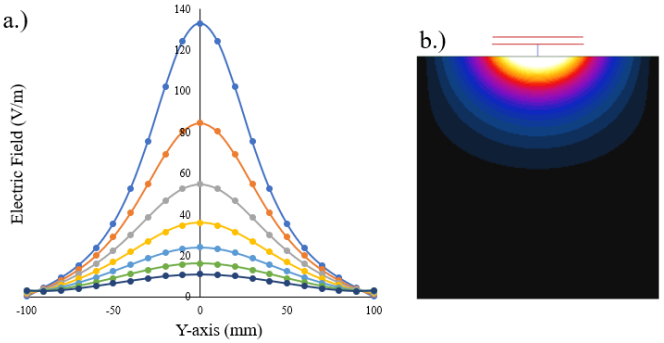

Fig. 9. a.) Electric field profile of the B65 coil in the Y-axis. b.) Slice view along the longitudinal plane of the gel phantom.

Additional simulations were run to compare the Magventure B65 coils, QBC and THC. The slice view of the induced electric field along the coronal plane at the origin is shown for the three coils in Fig. 10. We observe that at the origin, the QBC delivers stimulation at a higher electric field than the other two coils.

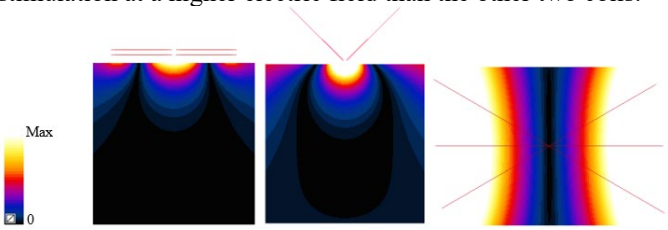

Fig. 10. Slice views of the induced electric field along the coronal plane at origin (0,0,0) for a.) B65 coil b.) QBC c.) THC. The views have been normalized with the maximum value of the induced electric field that the B65 coil induces in the brain.

Fig. 11 presents the induced electric field from the three coils at the location 40,0,0. This graph shows that at X = 40 mm, the induced electric field of the QBC and B65 coils begin to tend toward zero with increasing Z distance while the induced electric field of the THC increases with increasing Z distance

making the THC a good coil for achieving stimulation at greater depth.

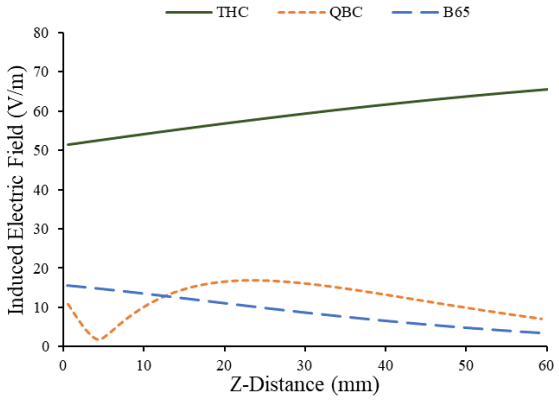

Fig. 11. Graph comparing the induced electric field of the three coils at location 40,0,0.

Another reading was extracted at the edge of the gel phantom at the point 100,0,0 and the result of the induced electric field is represented in Fig. 12. We also see that the THC induces a higher electric field at the edge of the phantom while the other two coils tend to zero. With this result, we confirm that the THC is a good coil when considering administering TMS at a greater depth.

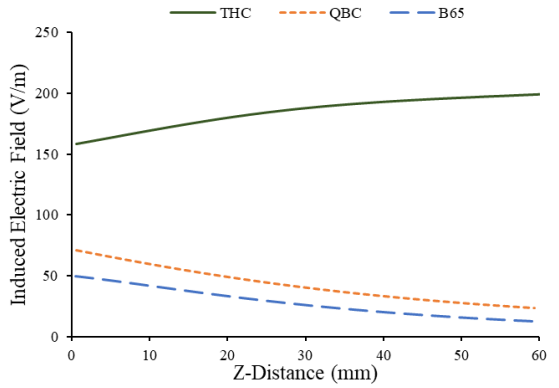

Fig. 12. Graph comparing the induced electric field of the three coils at location 100,0,0.

IV. Conclusion And Future Work

The simulation results presented in this research show good correlation with the induced voltage measurements. With the close fitting between the electric field and the induced voltage, the electric field intensity from electromagnetic modeling can be used to estimate the spatial distribution of the induced voltage within the gel phantom. These results serve as a base for future experiment and simulation and as an important information when administering TMS in humans with the novel coils. To further investigate our results, we intend to measure the electric field intensity in our gel phantom for a better comparison with simulation results using the methods mentioned in the work of [16], [17]. We also intend to sample more grid points (locations) in our future experiments so that effect of coil geometry and configuration can be observed.

Acknowledgment

This research was supported by the Iowa Seed Grant Program, Board of Regents, State of Iowa.

References

[1] M. Chen and D. J. Mogul, “A Structurally-Detailed Finite Element Human Head Model for Brain-Electromagnetic Field Simulations,” in *2007 3rd International IEEE/EMBS Conference on Neural Engineering*, May 2007, pp. 291–293, doi: 10.1109/CNE.2007.369668.

[2] A. Chail, R. K. Saini, P. S. Bhat, K. Srivastava, and V. Chauhan, “Transcranial magnetic stimulation: A review of its evolution and current applications,” *Ind. Psychiatry J.*, vol. 27, no. 2, pp. 172–180, 2018, doi: 10.4103/ipj.ipj_88_18.

[3] E. M. Wassermann and S. H. Lisanby, “Therapeutic application of repetitive transcranial magnetic stimulation: a review,” *Clin. Neurophysiol.*, vol. 112, no. 8, pp. 1367–1377, Aug. 2001, doi: 10.1016/S1388-2457(01)00585-5.

[4] E. M. Wassermann and T. Zimmermann, “Transcranial magnetic brain stimulation: Therapeutic promises and scientific gaps,” *Pharmacol. Ther.*, vol. 133, no. 1, pp. 98–107, Jan. 2012, doi: 10.1016/j.pharmthera.2011.09.003.

[5] Z.-D. Deng, S. H. Lisanby, and A. V. Peterchev, “Electric field depth–focality tradeoff in transcranial magnetic stimulation: Simulation comparison of 50 coil designs,” *Brain Stimulat.*, vol. 6, no. 1, pp. 1–13, Jan. 2013, doi: 10.1016/j.brs.2012.02.005.

[6] L. J. Crowther, P. Marketos, P. I. Williams, Y. Melikhov, D. C. Jiles, and J. H. Starzewski, “Transcranial magnetic stimulation: Improved coil design for deep brain investigation,” *J. Appl. Phys.*, vol. 109, no. 7, p. 07B314, Apr. 2011, doi: 10.1063/1.3563076.

[7] M. Lu and S. Ueno, “Deep Transcranial Magnetic Stimulation Using Figure-of-Eight and Halo Coils,” *IEEE Trans. Magn.*, vol. 51, no. 11, pp. 1–4, Nov. 2015, doi: 10.1109/TMAG.2015.2436977.

[8] P. I. Petrov, S. Mandija, I. E. C. Sommer, C. A. T. van den Berg, and S. F. W. Neggers, “How much detail is needed in modeling a transcranial magnetic stimulation figure-8 coil: Measurements and brain simulations,” *PLOS ONE*, vol. 12, no. 6, pp. 1–20, 2017, doi: 10.1371/journal.pone.0178952.

[9] P. Rastogi, E. G. Lee, R. L. Hadimani, and D. C. Jiles, “Transcranial Magnetic Stimulation-coil design with improved focality,” *AIP Adv.*, vol. 7, no. 5, p. 056705, May 2017, doi: 10.1063/1.4973604.

[10] P. Rastogi, E. G. Lee, R. L. Hadimani, and D. C. Jiles, “Transcranial Magnetic Stimulation: Development of a Novel Deep-Brain Triple-Halo Coil,” *IEEE Magn. Lett.*, vol. 10, pp. 1–5, 2019, doi: 10.1109/LMAG.2019.2903993.

[11] MagVenture, Inc., GA, USA. “Magnetic Stimulation Product Sheet” Accessed on: June 15, 2020. [Online]. Available: https://www.magventure.com/us/tms-research/products-overview/research-coils/coils/cool-bb65.

[12] “E. Neufeld, M. C. Gosselin, D. Sczcerba, M. Zefferer, and N. Kuster, “Sim4Life: A Medical Image Data Based Multiphysics.”

[13] B. W. Scandling, “Radio Frequency Induced Heating of a Medical Device with Vascular Flow Conditions,” p. 24.

[14] H. Moschiano, W. Dabney, R. S. Johnson, and L. Placek, “Thermal and Electrical Characterization of PAA and HEC Gel used in MRI Testing of Active and Passive Medical Implants”

[15] “AD-TECH Catalogue-2015.pdf.” Accessed: May 08, 2020. [Online]. Available: http://www.severnhealthcare.com/images/documents/ad-tech/AD-TECHCatalogue-2015.pdf.

[16] Nieminen JO, Koponen LM, Ilmoniemi RJ. Experimental Characterization of the Electric Field Distribution Induced by TMS Devices. Brain Stimul. 2015;8(3):582-589. doi:10.1016/j.brs.2015.01.004

[17] A. Zolj, S. N. Makarov, L. Navarro de Lara and A. Nummenmaa, "Electrically Small Dipole Antenna Probe for Quasistatic Electric Field Measurements in Transcranial Magnetic Stimulation," in IEEE Transactions on Magnetics, vol. 55, no. 1, pp. 1-10, Jan. 2019, Art no. 5800110, doi: 10.1109/TMAG.2018.2875882.